Supporting Information:

Synthesis of a Bimetallic Dodecaborate $LiNaB_{12}H_{12}$ with Outstanding Super Ionic Conductivity

Liqing He,[†] Hai-Wen Li,[, ‡§] Hironori Nakajima,[†§] Nikolay Tumanov,[⊥] Yaroslav Filinchuk,[*, ⊥] Son-Jong Hwang,[#] Manish Sharma,[∥] Hans Hagemann,[∥] and Etsuo Akiba[†‡§]*

† Department of Mechanical Engineering, Kyushu University, Fukuoka 819-0395, Japan

‡ International Research Center for Hydrogen Energy, Kyushu University, Fukuoka 819-0395, Japan

§ WPI International Institute for Carbon-Neutral Energy Research (WPI-I2CNER), Kyushu University, Fukuoka 819-0395, Japan

⊥ Institute of Condensed Matter and Nanosciences, Université Catholique de Louvain, Louvain-la-Neuve 1348, Belgium

Division of Chemistry and Chemical Engineering, California Institute of Technology, Pasadena, California 91125, USA

∥ Département de Chimie Physique, Université de Genève, 30, quai E. Ansermet, 1211 Geneva 4, Switzerland

***Corresponding Author:**

* (H.L.) E-mail: li.haiwen.305@m.kyushu-u.ac.jp.

* (Y.F.) E-mail: Yaroslav.Filinchuk@uclouvain.be.

Sample Synthesis

Commercial $B_{10}H_{14}$ (99%, Wako), $LiBH_4$ (95%, Aldrich), $NaBH_4$ (99.99%, Aldrich) were all stored in glove box and used without further purification. Mechanical milling was carried out using Fritsch P-7 ball milling machine. Starting materials $LiBH_4$ + $NaBH_4$ + $B_{10}H_{14}$ (1:1:1 in mole rate) was firstly mechanically milled at room temperature using planetary ball mill (Fritsch P-7) with 10 steel balls (7 mm in diameter) in a hardened steel vial (30 cm^3 in volume) under 0.1 MPa Ar for 5 h (15 min milling, 5 min pausing). Subsequently, the ball milled products were sealed into (~0.7 cm^3) stainless steel crucibles for heat treatment at 673 K with 10 h.

Characterization

Powder X-ray diffraction (XRD) patterns were recorded using Rigaku Ultima IV X-ray diffractometer with Cu-Kα radiation using 40 kV/ 40 mA as accelerating voltage/ tube current. The sample powders were placed in a glass plate sealed by Scotch tape to avoid air exposure during the measurement. Raman and In-situ Raman spectra were examined by RAMAN-11 VIS-SS (Nanophoton) using a green laser with a wavelength of 532 nm. Solid-state magic angle spinning (MAS) nuclear magnetic resonance (NMR) spectra were recorded using a Bruker DSX-500 spectrometer and a boron background free 4 mm Bruker MAS probe at room temperature. NMR sample preparations were always handled in a glove box filled with purified Ar gas and dry N_2 gas was used for sample spinning. ^{11}B MAS NMR spectra were obtained after a short pulse (0.5 μs – π/12 pulse) and with strong ^{1}H decoupling pulses, indicating the purity for $B_{12}H_{12}$ species is approximately 86%, and the remained 14% are assigned as the impurity of $B_{10}H_{10}$ species. ^{11}B NMR chemical shifts were referenced to BF_3OEt_2 (δ = 0.00 ppm).

Differential scanning calorimetry profiles are examined by Thermo plus2 DSC8230HP AEMK under 0.1 MPa He with a gas flow rate of 200 ml/min.

High-resolution X-ray powder diffraction patterns were measured at variable temperature using a synchrotron radiation source at BM1A station at the Swiss-Norwegian Beam Lines at the ESRF (λ = 0.68857 and 0.698509 Å, Pilatus 2M hybrid pixel detector). Nominal sample-to-detector distances (344 mm), coordinates of beam center and detector tilts were calibrated using LaB_6 (NIST standard 660b). A powdered sample of $LiNaB_{12}H_{12}$ was filled in the sapphire single crystal capillary for the experiment with H_2 pressure and in the quartz capillary for the experiment without pressure load. All manipulations were done in the argon-filled glove box ($p(O_2, H_2O)$ < 1 ppm). First capillary was placed in a specially developed *in situ* sample cell for investigation of solid-gas reactions. [1] The samples were heated with a rate of 5 K/min between RT and 623 K in p(Ar) ≈ 1 bar and $p(H_2)$ ≈ 160 bar. Raw powder diffraction data were processed (calibration, integration) using the Fit2D program. [2] Uncertainties of the integrated intensities were calculated at each 2θ-point by applying Poisson statistics to the intensity data, considering the geometry of the 2D detector. [3,4] The structures were refined by the Rietveld method using a Fullprof Suite software. [5] The final refinement of $LiNaB_{12}H_{12}$ low temperature phase was done in *Pa*-3 space group .The background was described by linear interpolation between selected points. The final discrepancy factors are: R_B = 6.10%, R_F = 9.50%, R_p = 10.0%, and R_{wp} = 9.97% (corrected for background). The refinement profile is shown in Fig. S3. Crystal data and atomic coordinates are listed in Table S1. High temperature phase of $LiNaB_{12}H_{12}$ was modeled in *Fm*-3*m* space group, Z= 4, a = 9.82707(9) Å, V = 1040.204(11) $Å^3$at 513 K. Li and Na are located on *x*, *x*, *x* position (x =0.29683),

centered around the 8-fold 1/4 1/4 1/4 position, and the presumably disordered dodecabotate is located near the 0, 0, 0 position. The final discrepancy factors are: R_B = 1.55%, R_F = 12.7%, R_p = 9.10%, and R_{wp} = 6.74% (corrected for background). The refinement profile is shown in Fig. S4.

Ionic conductivities were measured with electrochemical impedance spectroscopy [6] for the sample pressed into a pellet with a diameter of 8 mm and a thickness of approximately 2 mm. Cu foils with a thickness of 20 μm were used as electrodes, which were mechanically fixed on both sides of the pellet sample in an air-tight cell (Hohsen, HS-cell). Impedance plots shown in Fig. S5 were measured at the open circuit potential between 300 and 550 K using a frequency response analyzer (Ono Sokki, DS-2100/DS-266/DS-273) combined with a potentio/galvanostat (Hokuto Denko, HA-301) in a frequency range from 0.1 MHz to 1 Hz. Ionic conductivities of the sample were derived from the high frequency resistances obtained by the complex nonlinear least-squares fitting (Scribner, Z-View) for the impedance spectra. [6] The spectra did not exhibit clear separation of overlapping contributions of the bulk and grain boundary. All the sample preparations and the air-tight cell assembly were always handled in a glove box filled with purified Ar gas. Transport number of Lithium ion was measured by potentiostatic polarization measurement using Li foils with a thickness of 100 μm as electrodes. [7,8] Time variations of the current were recorded by a data logger (GRAPHTEC, midi LOGGER GL820) for the sample sandwiched by Li foil electrodes with a thickness of 100 μm in the air-tight cell under constant potential differences with time applied between the electrodes by the potentio/galvanostat. Fig. 6S shows the current transient, where the initial and steady-state currents, i_0 and i_∞, respectively, give the transport number of Li ion, $t_{Li,}$ from the following equation with the constant

potential differences of ΔV. [7,8]

$$t_{Li^+} = \frac{\Delta V/i_0 - R_{ct}}{\Delta V/i_\infty - R_{ct}}$$

where the charge transfer resistance, R_{ct}, assumed constant with time was negligibly small compared with the other resistances in the impedance spectra for the sample with the Li electrodes.

Computational studies were performed with the Gaussian 09 program using Density Functional Theory (DFT) with the B3LYP functional and 6-31G(d,p) basis set. [9]

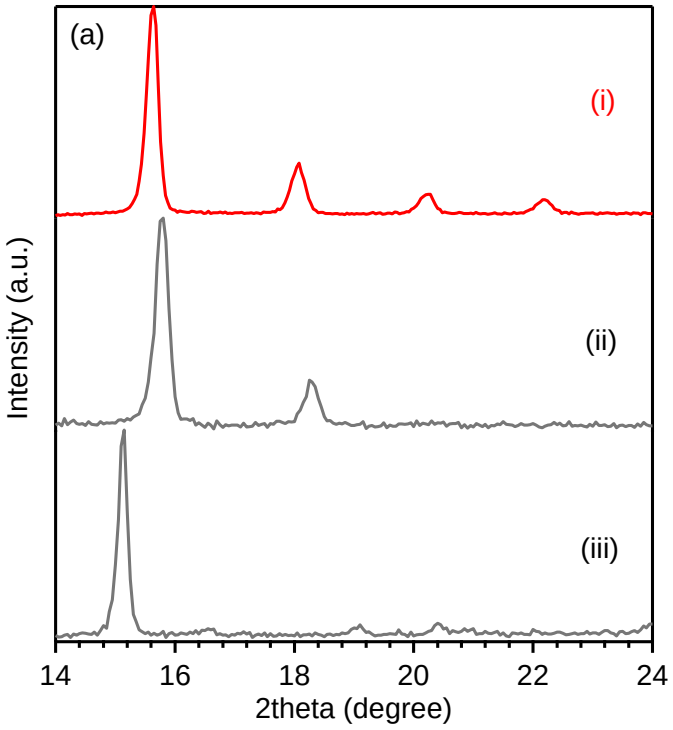

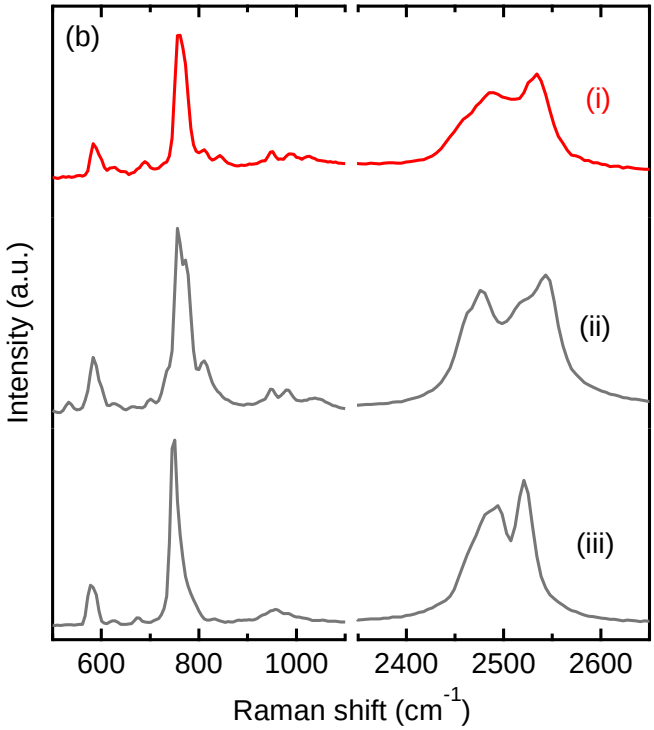
(b)
(i)
(ii)
(iii)
Intensity (a.u.)
600
800
1000
2400
2500
2600
Raman shift (cm-1)

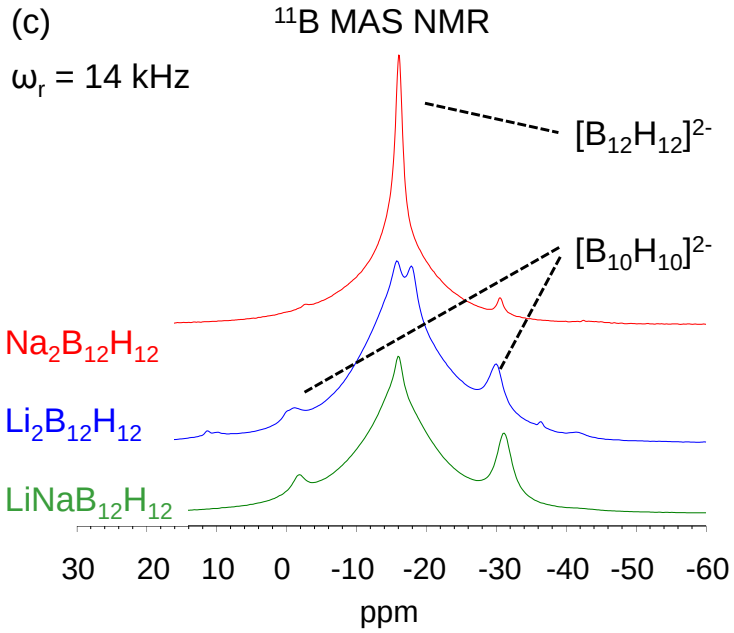
(c)
11B MAS NMR
ωr = 14 kHz
[B12H12]2-
[B10H10]2-
Na2B12H12
Li2B12H12
LiNaB12H12
30
20
10
0
-10
-20
-30
-40
-50
-60
ppm

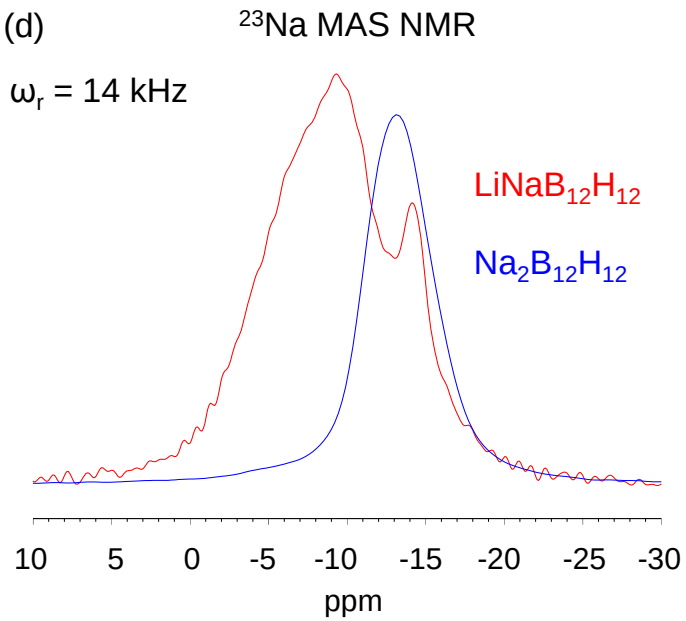

Fig. S1 (a) XRD diffraction patterns, (b) Raman spectra, (c) ^{11}B and (d) ^{23}Na MAS NMR profiles of (i) 5 h ball milled $LiBH_4$ + $NaBH_4$ + $B_{10}H_{14}$ followed by heat treatment at 673 K for 10 h; (ii) $Li_2B_{12}H_{12}$ and (iii) $Na_2B_{12}H_{12}$.

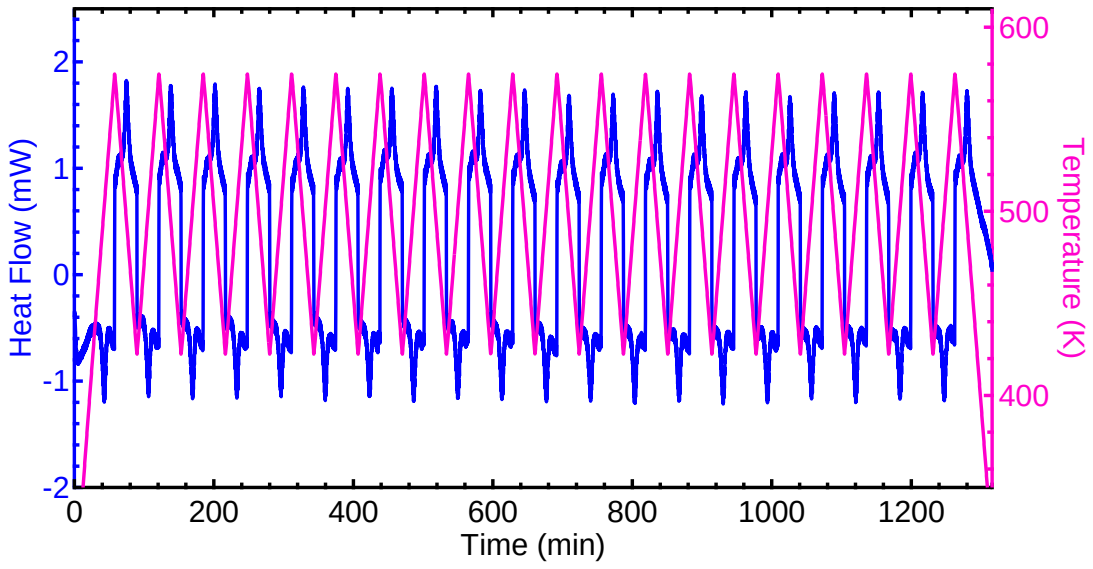

Fig. S2 DSC measurement of $LiNaB_{12}H_{12}$ between 423 and 573 K for 20 cycles (5 K /min in 0.1 MPa He).

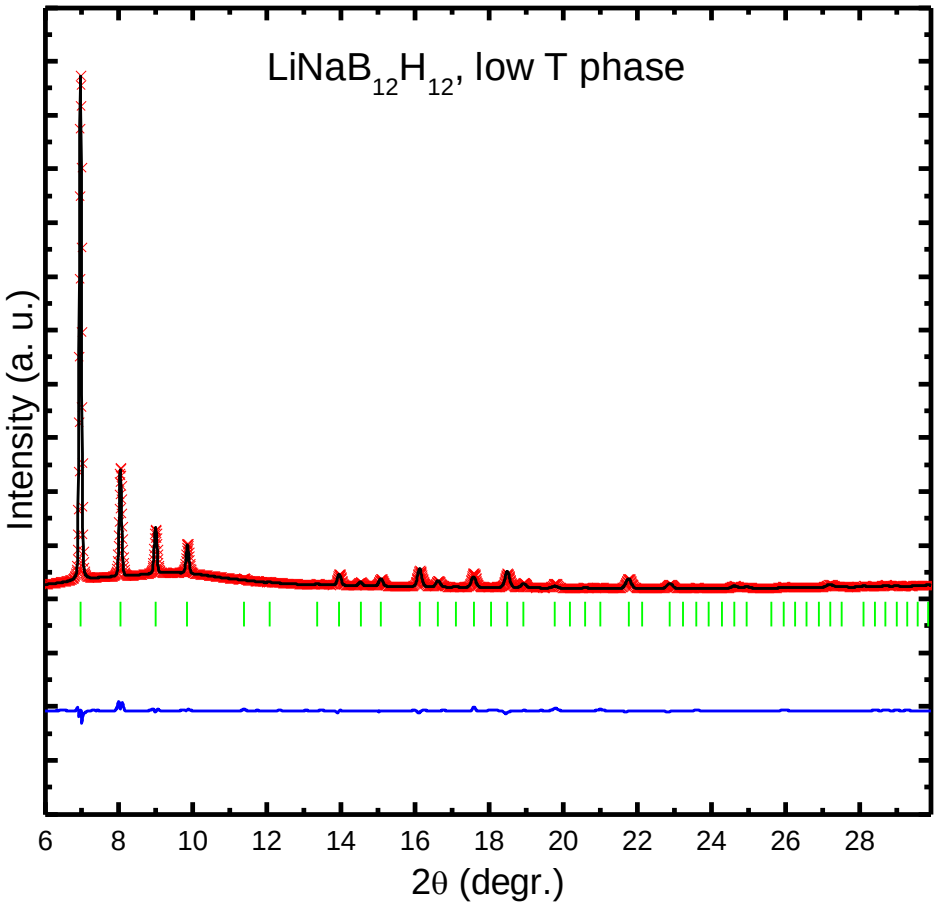

Figure S3 Rietveld refinement plot for $LiNaB_{12}H_{12}$ at 303 K (low temperature phase). Red crosses and black line show the experimental and calculated data, respectively. Blue line is the difference profile, and green marks indicate Bragg positions. λ = 0.68857 Å.

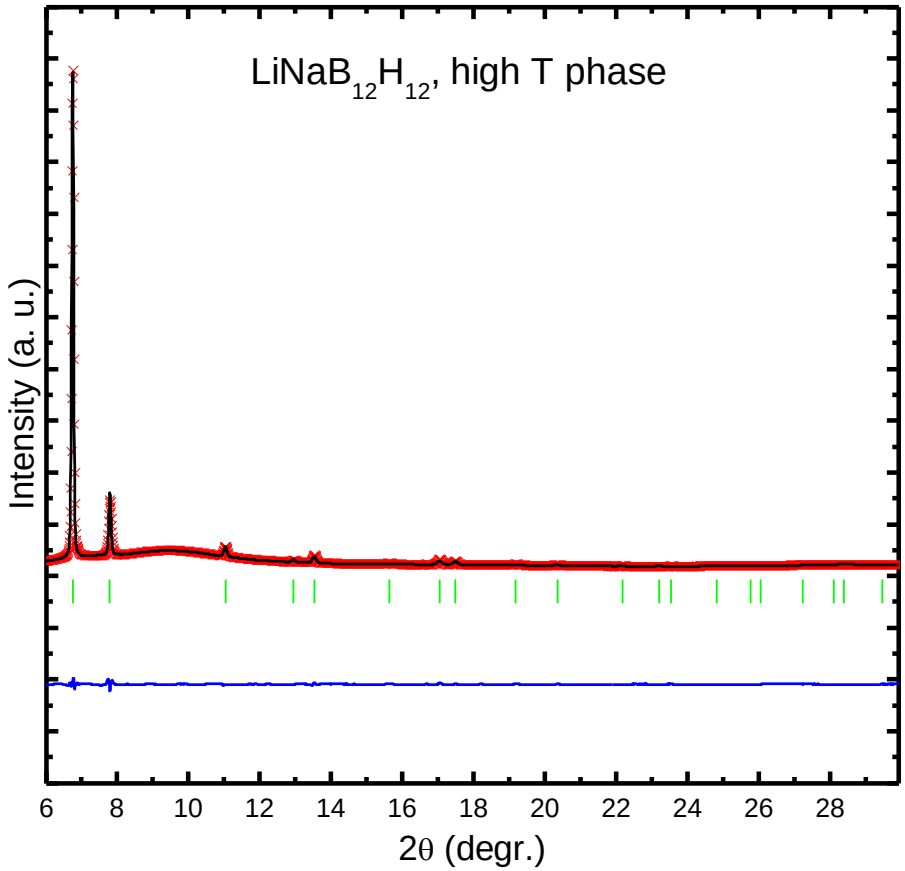

Figure S4 Rietveld refinement plot for $LiNaB_{12}H_{12}$ at 513 K (high temperature phase). Red crosses and black line show the experimental and calculated data, respectively. Blue line is the difference profile, and green marks indicate Bragg positions. $\lambda = 0.68857$ Å.

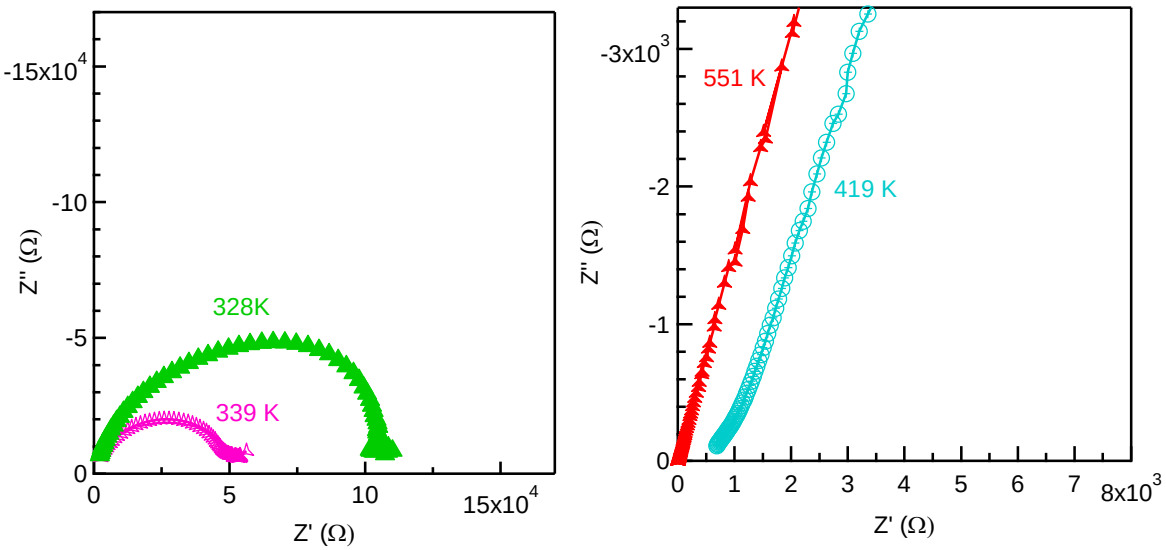

Fig. S5 Impedance plots for $LiNaB_{12}H_{12}$ measured at various temperatures during heating run.

(a)

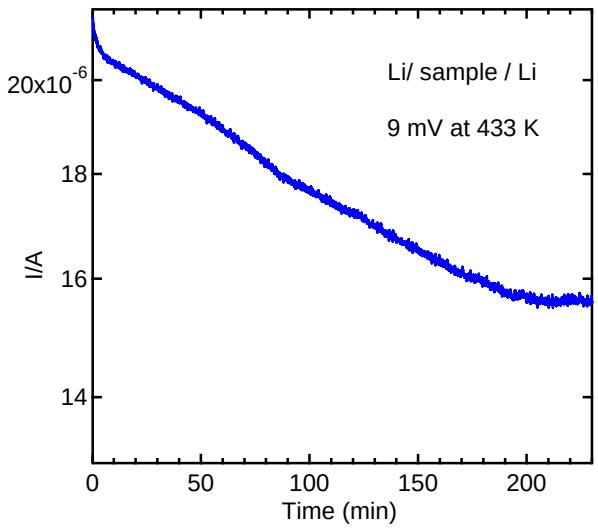

(b)

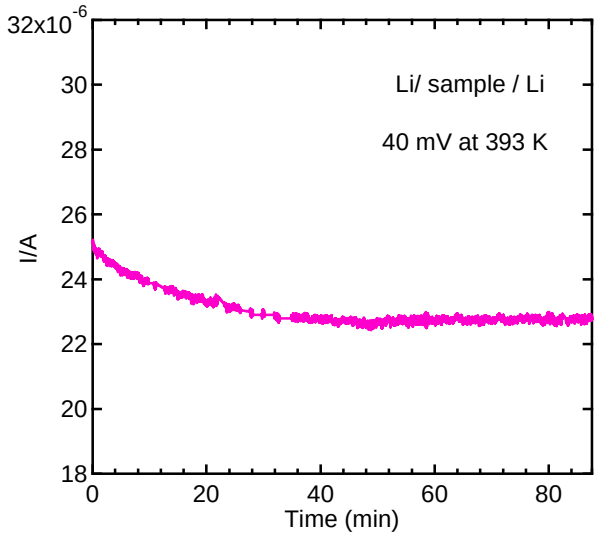

Fig. S6 Time variation of the current with the potentiostatic polarization of a Li|LiNa$B_{12}H_{12}$|Li cell at (a) 433 K and (b) 393 K and applied potential difference of 9 mV and 40 mV, respectively.

Table S1 Experimental structural parameters for $LiNaB_{12}H_{12}$ at 303 K (low temperature phase). Space group*Pa*-3, Z = 4, a = 9.82707(9) Å, V = 949.01(3) $Å^3$. The refined fractional site occupancy for Na1 is 0.377, for Li 0.623, close to the nominal composition (0.5/0.5), all other atoms fully occupy their crystallographic positions.

Atom	**x**	**y**	**z**
Li1	0.63644	0.63644	0.63644
Na1	0.63644	0.63644	0.63644
B1	-0.09125	-0.09102	0.12363
B2	-0.03597	-0.03888	-0.17056
H1	-0.15556	-0.15515	0.21074
H2	-0.06132	-0.06628	-0.29074

Table S2 Calculated vibrational frequencies for isolated $B_{12}H_{12}^{2-}$ and $Li_2B_{12}H_{12}$ (molecule with D_{3d} symmetry) and experimental vibrational frequencies for solid $Cs_2B_{12}H_{12}$ [10] and $LiNaB_{12}H_{12}$ [this work]. In I_h symmetry, A_g and H_g are Raman active, and T_{1u} IR active. In D_{3d} symmetry, A_{1g} and E_g are Raman active, and A_{2u} and E_u IR active.

$B_{12}H_{12}$ calc DFT	I_h	$Cs_2B_{12}H_{12}$ Allis		$Li_2B_{12}H_{12}$ calc DFT	D_{3d}	Raman $LiNaB_{12}H_{12}$
				223,223, 259,260 436, 475 (Li)		
516 (x5)	H_u	531		514, 514, 523 545, 545	$A_{1u} + 2E_u$	
572 (x5)	H_g	581 (R) 586 (R)		564, 565 579,580 619	$A_{1g} + 2E_g$	579 618
652 (x4)	G_g			655 662 (A_{2g}) 671 672	$A_{1g} + A_{2g} + E_g$	679

702 (x3)	T_{1u}	708,718		707 722, 722	$A_{2u} + E_u$	
734 (x4)	G_u	757		725, 743, 743 754	$A_{1u} + A_{2u} + E_u$	
737 (x1)	A_g	747		749	A_{1g}	751
753 (x5)	H_g	762 787		761,761, 795, 795 830	$A_{1g} + 2E_g$	801 834
758 (x3?)	T_{2u}			792, 792 811	$A_{2u} + E_u$	
862 (x4)	G_u	860		857 (A_{1u}) 872, 872, 944	$A_{1u} + A_{2u} + E_u$	
937 (x4)	G_g	940		930,930 939 955	$A_{1g} + A_{2g} + E_g$	942
941 (x5)	H_u	950		945, 946 950 998,998	$A_{1u} + 2E_u$	
943 (x5)	H_g	972		946 947, 947 962,963	$A_{1g} + 2E_g$	979
957 (x3)	T_{1g}			1025, 1069,1069	$A_{2g} + E_g$	
1063 (x3)	T_{1u}	1057 1073		1089 1124, 1124	$A_{2u} + E_u$	
2476 (x3)	T_{2u}			2421, 2421 2446	$A_{2u} + E_u$	
2483 (x5)	H_g			2420, 2420 2455 2635,2635	$A_{1g} + 2E_g$	2485
2504 (x3)	T_{1u}			2632 2642,2642	$A_{2u} + E_u$	
2542 (x1)	A_g			2650	A_{1g}	2525

Table S3 Correlation table for selected subgroups of I_h

I_h	T_h	T	D_{2h}	D_{3d}	C_{3v}	D_{5d}	C_{5v}
A_g	A_g	A	A_g	A_{1g}	A_1	A_{1g}	A_1
T_{1g}	T_g	T	B_{1g} +B_{2g} + B_{3g}	A_{2g} + E_g	A_2 + E	A_{2g} + E_{1g}	A_2 + E_1
T_{2g}	T_g	T	B_{1g} +B_{2g} + B_{3g}	A_{2g} + E_g	A_2 + E	A_{2g} + E_{2g}	A_2 + E_1
G_g	A_g + T_g	A + T	A_g + B_{1g} +B_{2g} + B_{3g}	A_{1g} + A_{2g} + E_g	A_1 + A_2 + E	E_{1g} + E_{2g}	E_1 + E_2
H_g	E_g +T_g	E + T	2A_g + B_{1g} +B_{2g} + B_{3g}	A_{1g} + 2E_g	A_1 + 2E	A_{1g} + E_{1g} + E_{2g}	A_1 + E_1 + E_2
A_u	A_u	A	A_u	A_{1u}	A_2	A_{1u}	A_2
T_{1u}	T_u	T	B_{1u} + B_{2u} + B_{3u}	A_{2u} + E_u	A_1 + E	A_{2u} + E_{1u}	A_1 + E_1
T_{2u}	T_u	T	B_{1u} + B_{2u} + B_{3u}	A_{2u} + E_u	A_1 + E	A_{2u} + E_{2u}	A_1 + E_1
G_u	A_u + T_u	A + T	A_u + B_{1u} + B_{2u} + B_{3u}	A_{1u} + A_{2u} + E_u	A_1 + A_2 + E	E_{1u} + E_{2u}	E_1 + E_2
H_u	E_u + T_u	E + T	2A_u + B_{1u} + B_{2u} + B_{3u}	A_{1u} + 2E_u	A_2 + E + E	A_{1u} + E_{1u} + E_{2u}	A_2 + E_1 + E_2

References:

(1) Jensen, T. R.; Nielsen, T. K.; Filinchuk, Y.; Jørgensen, J.-E.; Cerenius, Y.; Gray, E. M.; Webb, C. J. Versatile in situ powder X-ray diffraction cells for solid-gas investigations. *J. Appl. Crystallogr.* **2010**, *43*, 1456–1463.

(2) Hammersley, A. P.; Svensson, S. O.; Hanfland, M.; Fitch, A. N.; Hausermann, D. Two-dimensional detector software: from real detector to idealised image or two-theta scan. *High Press. Res.* **1996**, *14*, 235–248.

(3) Dyadkin, V. SNBL Tool box, Release 2013-1, Swiss Norwegian Beam Lines at ESRF, Grenoble, France **2013**.

(4) Vogel, S.; Ehm, L.; Knorr, K.; Braun, G. Automated processing of 2D powder diffraction data. *Adv. X-ray Anal.* **2002**, *45*, 31–33.

(5) Rodríguez-Carvajal, J. Recent advances in magnetic structure determination by neutron powder diffraction. *Phys. B Condens. Matter.* **1993**, *192*, 55–69.

(6) Barsoukov, E.; Macdonald, J. R. *Impedance Spectroscopy: Theory, Experiment, and Applications*, 2nd ed., John Wiley & Sons, New York: **2005**.

(7) Evans, J.; Vincent, C. A.; Bruce, P. G. Electrochemical measurement of transference numbers in polymer electrolytes. *Polymer* **1987**, *28*, 2324-2328.

(8) Watanabe, M.; Nagano, S.; Sanui, K.; Ogata, N. Estimation of Li^+ transport number in polymer electrolytes by the combination of complex impedance and potentiostatic polarization measurements. *Solid State Ionics* **1988**, *28–30*, 911-917.

(9) Frisch, M. J.; Trucks, G. W.; Schlegel, H. B.; Scuseria, G. E.; Robb, M. A.; Cheeseman, J. R.; Scalmani, G.; Barone, V.; Mennucci, B.; Petersson, G. A.; Nakatsuji, H.; Caricato, M.; Li, X.; Hratchian, H. P.; Izmaylov, A. F.; Bloino, J.; Zheng, G.; Sonnenberg, J. L.; Hada, M.; Ehara, M.; Toyota, K.; Fukuda, R.; Hasegawa, J.; Ishida, M.; Nakajima, T.; Honda, Y.; Kitao, O.; Nakai, H.; Vreven, T.; Montgomery Jr., J. A.; Peralta, J. E.; Ogliaro, F.; Bearpark, M. J.; Heyd, J.; Brothers, E. N.; Kudin, K. N.; Staroverov, V. N.; Kobayashi, R.; Normand, J.; Raghavachari, K.; Rendell, A. P.; Burant, J. C.; Iyengar, S. S.; Tomasi, J.; Cossi, M.; Rega, N.; Millam, N. J.; Klene, M.; Knox, J. E.; Cross, J. B.; Bakken, V.; Adamo, C.; Jaramillo,

J.; Gomperts, R.; Stratmann, R. E.; Yazyev, O.; Austin, A. J.; Cammi, R.; Pomelli, C.; Ochterski, J. W.; Martin, R. L.; Morokuma, K.; Zakrzewski, V. G.; Voth, G. A.; Salvador, P.; Dannenberg, J. J.; Dapprich, S.; Daniels, A. D.; Farkas, Ö.; Foresman, J. B.; Ortiz, J. V.; Cioslowski, J.; Fox, D. J. *Gaussian 09*, Gaussian, Inc.: Wallingford, CT, USA, **2009**.

(10) Allis, D.G.; Hudson, B.S. Inelastic neutron scattering spectrum of $Cs_2[B_{12}H_{12}]$: reproduction of its solid-state vibrational spectrum by periodic DFT. *J. Phys. Chem. A* **2006**, *110*, 3744-3749.